

## **Predicting the Structure of the Solar Corona During the 11 August 1999 Total Solar Eclipse**

Zoran Mikić, Jon A. Linker, Pete Riley, and Roberto Lionello

*Science Applications International Corporation, 10260 Campus Point  
Drive, San Diego, California 92121, U.S.A.*

**Abstract.** We describe the application of a three-dimensional magnetohydrodynamic (MHD) model to the prediction of the structure of the corona during the total solar eclipse of 11 August 1999. The calculation uses the observed photospheric radial magnetic field as a boundary condition. This model makes it possible to determine the large-scale structure of the magnetic field in the corona, as well as the distribution of the solar wind velocity, plasma density, and temperature. The density was used to predict the plane-of-sky polarization brightness prior to the eclipse. The prediction is compared with an eclipse image taken in Turkey.

### **1. Introduction**

Total solar eclipses offer an excellent opportunity to observe coronal streamers. During a total solar eclipse the moon blocks the bright light from the solar disk, so that the faint light scattered by the solar corona, which is more than a million times fainter than the photosphere, becomes visible. During totality the structures that characterize the white-light corona become visible, including prominences, helmet streamers, polar plumes, and coronal holes. Observers who witness a total solar eclipse invariably report that it is a beautiful sight to behold.

On 11 August 1999 a total solar eclipse occurred in Europe, the Middle East, and India. A partial eclipse was visible from the North-Eastern United States, and many parts of Europe, North Africa, and West Asia. (For an archive of past and future eclipse paths, see Fred Espenak's NASA eclipse home page.<sup>1</sup>) Fortunately, the viewing conditions were excellent in Harput, in Eastern Turkey, where one of us (ZM) successfully observed the eclipse.

In this paper we describe the a method of predicting the structure of the solar corona using a magnetohydrodynamic (MHD) model. By using this model it is possible to calculate the density in the corona, and thereby to deduce the brightness of coronal structures, given the observed magnetic field in the photosphere (a quantity that is measured routinely by several ground-based observatories). A description of the MHD model, as well as its application to the prediction of the structure of the corona during eclipses, is given by Mikić et al. (1999).

---

<sup>1</sup>See: <http://sunearth.gsfc.nasa.gov/eclipse/eclipse.html>

Previous comparisons of our results with coronal and interplanetary observations have shown that the large-scale structure of the solar corona is largely determined by the photospheric magnetic field distribution. It is remarkable that an MHD model, which incorporates the balance of magnetic, plasma, and gravity forces in equilibrium, can be used to estimate the large-scale distribution of plasma, magnetic field, and solar wind in the corona, using only the measured magnetic field in the photosphere.

This model can be used to make a prediction of the structure of the corona prior to eclipse day by using synoptic magnetic field measurements taken from the preceding solar rotation. After the calculation is performed, the white-light polarized brightness of the corona can be simulated from the MHD solution by integrating the electron density along the line of sight in the plane of the sky. This image can then be compared with coronal images taken during the eclipse. We published our prediction on the World Wide Web on 4 August 1999 (<http://haven.saic.com/corona/modeling.html>). Our prediction was updated and finalized on 6 August 1999, five days prior to the eclipse.

## 2. The MHD Model

Over the past decade we have developed a 3D MHD model of the corona and inner heliosphere. At present, we primarily use a polytropic MHD model for our large-scale calculations. This model, briefly described here, relies on a simple form of the energy equation (an adiabatic fluid with a reduced polytropic index). A more sophisticated model incorporating a more realistic description of the energy flow in the corona (including thermal conduction parallel to the magnetic field, radiation loss, coronal heating, and Alfvén wave acceleration) is under development (Mikić et al. 1999), and will be used in the future to improve our description of the corona and solar wind.

In the polytropic MHD model, the coronal plasma is described by the following equations:

$$\nabla \times \mathbf{B} = \frac{4\pi}{c} \mathbf{J}, \quad (1)$$

$$\nabla \times \mathbf{E} = -\frac{1}{c} \frac{\partial \mathbf{B}}{\partial t}, \quad (2)$$

$$\mathbf{E} + \frac{1}{c} \mathbf{v} \times \mathbf{B} = \eta \mathbf{J}, \quad (3)$$

$$\frac{\partial \rho}{\partial t} + \nabla \cdot (\rho \mathbf{v}) = 0, \quad (4)$$

$$\rho \left( \frac{\partial \mathbf{v}}{\partial t} + \mathbf{v} \cdot \nabla \mathbf{v} \right) = \frac{1}{c} \mathbf{J} \times \mathbf{B} - \nabla p + \rho \mathbf{g} + \nabla \cdot (\nu \rho \nabla \mathbf{v}), \quad (5)$$

$$\frac{\partial p}{\partial t} + \nabla \cdot (p \mathbf{v}) = -(\gamma - 1)p \nabla \cdot \mathbf{v}, \quad (6)$$

where  $\mathbf{B}$  is the magnetic field,  $\mathbf{J}$  is the electric current density,  $\mathbf{E}$  is the electric field,  $\rho$ ,  $\mathbf{v}$ ,  $p$ , and  $T$  are the plasma mass density, velocity, pressure, and temperature,  $\mathbf{g}$  is the gravitational acceleration,  $\gamma$  is the polytropic index,  $\eta$  is the

resistivity, and  $\nu$  is the kinematic viscosity. The plasma pressure is  $p = 2nkT$ , where  $n$  is the electron and proton density, which are assumed to be equal. In the polytropic model, the complicated energy flow in the corona is modeled with a simple adiabatic energy equation with reduced  $\gamma$  (i.e., smaller than  $5/3$ ; see Parker 1963). The primary motivation for using a reduced  $\gamma$  is the fact that the temperature in the corona does not vary substantially (the limit  $\gamma \rightarrow 1$  corresponds to an isothermal plasma). A typical choice, used here, is  $\gamma = 1.05$ .

We have developed a three-dimensional code to solve equations (1)–(6) in spherical coordinates  $(r, \theta, \phi)$  (Mikić & Linker 1994; Lionello, Mikić, & Schnack 1998). This code has been used extensively to model the 2D and 3D corona, including the structure of helmet streamers (Mikić & Linker 1996; Mikić, Linker & Schnack 1996; Linker et al. 1999), coronal mass ejections (Mikić & Linker 1994; Linker, Mikić, & Schnack 1994; Linker & Mikić 1995; Mikić & Linker 1997; Linker & Mikić 1997), and the long-term evolution of the solar corona and heliospheric current sheet (Mikić et al. 1999). Related techniques have been developed by Pneuman and Kopp (1971), Endler (1971), Steinolfson et al. (1982), Washimi, Yoshino, and Ogino (1987), Wang et al. (1993), Usmanov (1993, 1999), and Suess et al. (1999).

A boundary condition is imposed on the radial component of the magnetic field,  $B_r$ , at the lower corona ( $r = R_s$ ). We use synoptic maps of the line-of-sight photospheric magnetic field measured at the National Solar Observatory at Kitt Peak (NSOKP) for this purpose. These photospheric magnetic field maps are built up from daily observations of the Sun during a solar rotation, and give a good approximation of the Sun's magnetic flux if the large-scale flux does not change considerably over a rotation. We also specify a uniform plasma density ( $n_0 = 2 \times 10^8 \text{ cm}^{-3}$ ) and temperature ( $T_0 = 1.8 \times 10^6 \text{ K}$ ) at  $r = R_s$  in regions where the radial velocity is positive.

The application of the model is described by Mikić et al. (1999). Briefly, we start with a potential field in the corona (with  $\nabla \times \mathbf{B} = 0$ ) that matches the measured field  $B_r$  at the base of the corona, and a transonic spherically symmetric solar wind solution (Parker 1963) to specify  $p$ ,  $\rho$ , and  $\mathbf{v}$ . This initial nonequilibrium field is integrated in time until a steady state is reached. The final state has closed magnetic field regions (helmet streamers), where the solar wind plasma is trapped, surrounded by open fields (coronal holes), where the solar wind flows freely along magnetic field lines, accelerating to supersonic speeds.

### 3. The Prediction

Previous applications of our model to the prediction of the state of the solar corona were performed for eclipses that occurred close to solar minimum: the 3 November 1994 eclipse<sup>2</sup>, which occurred during the declining phase of the last solar cycle; the 24 October 1995 and 9 March 1997 eclipses, which occurred at solar minimum, and the 26 February 1998 eclipse, which occurred during the

---

<sup>2</sup>We did not make a prediction for the 1994 eclipse. However, we compared eclipse images with a coronal model after the eclipse.

early rising phase of the new solar cycle. The 11 August 1999 eclipse presented a new challenge to our modeling efforts because it occurred during the late rising phase of the solar cycle on the approach to solar maximum. During this time, the solar magnetic field is significantly more complex than during solar minimum. The number of active regions is much larger, and the streamer structure in the corona is considerably more complex. A consequence for numerical modeling is the need for a significantly larger number of mesh points in the calculation to resolve coronal structures. Whereas our solar minimum calculations were performed on  $(r, \theta, \phi)$  grids with  $81 \times 81 \times 64$  mesh points, in the present calculation we use  $111 \times 141 \times 128$  mesh points. In addition, the large-scale magnetic field strength is larger, requiring smaller time steps. These calculations therefore took significantly longer to perform (90 CPU hours on a single processor of the T90 Cray supercomputer). We are presently developing a massively parallel version of our code which will enable us to perform these calculations in less time.

Using magnetic field measurements from a previous solar rotation for a prediction is expected to be a poorer approximation during this phase of the solar cycle than during solar minimum, when the large-scale structure of the Sun changes slowly between solar rotations. The photospheric magnetic field evolves more rapidly, making synoptic magnetic field measurements a less reliable approximation to the true state of the photospheric magnetic field. Figure 1 shows the evolution of the NSOKP photospheric magnetic field synoptic maps during the four solar rotations preceding the eclipse. Note that there is significant evolution of the magnetic field from rotation to rotation as active regions emerge and disperse. Figure 2 shows a comparison of a NSOKP synoptic map from June–July, 1999 with one near solar minimum (August–September, 1996), showing that the photospheric magnetic field is considerably more complex now. Consequently, the coronal magnetic field would be expected to be significantly more complex also. This expectation is confirmed by our results, described below.

The magnetic field is fitted at the solar poles using a smoothing procedure, since the line-of-sight component is not measured accurately there due to projection effects. Additionally, the data is smoothed everywhere, since the spatial resolution of the calculation is less than that of the measurements. The poor accuracy of the polar field (a limitation of the measurements) is expected to compromise our prediction more severely at this time of high solar activity, when active regions and coronal streamers are found at high latitudes, than at solar minimum.

On 28 July 1999 we started an MHD computation to predict the structure of the solar corona during the 11 August 1999 eclipse. We used NSOKP photospheric magnetic field measurements from Carrington rotation 1951 (corresponding to the dates 24 June–21 July, 1999). Figure 3 shows the raw NSOKP data and the smoothed data used in our calculation. It is apparent that the large-scale features in the magnetic field are reasonably well represented by the smoothed field.

Once the coronal solution reaches equilibrium, we use the density from the calculation to simulate the white-light polarized brightness of the corona on eclipse day. The polarized brightness is computed by integrating the electron

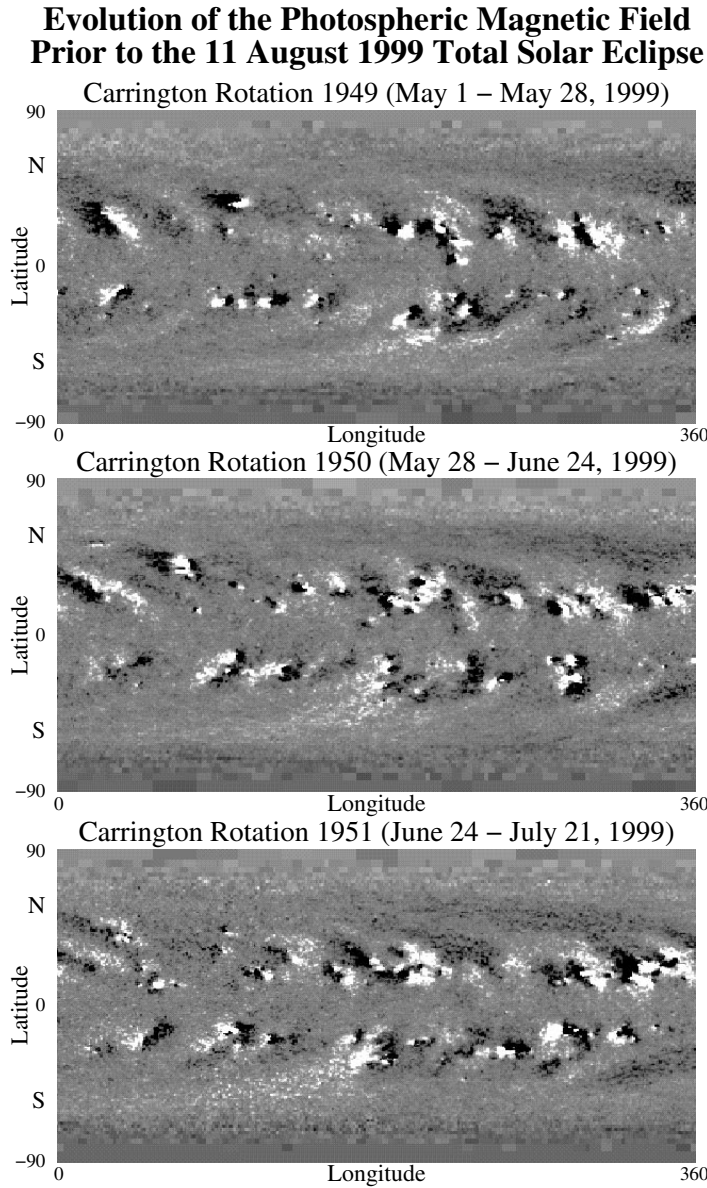


Figure 1. Synoptic maps of the radial component of the photospheric magnetic field for three solar rotations (Carrington rotations 1949–1951), as measured at the National Solar Observatory at Kitt Peak. Black shows fields directed into the Sun, whereas white shows fields directed out of the Sun. These maps show that the magnetic field is changing rapidly during the approach to the eclipse of 11 August 1999.

### Comparison of Photospheric Magnetic Fields: Near Solar Minimum and Approaching Solar Maximum

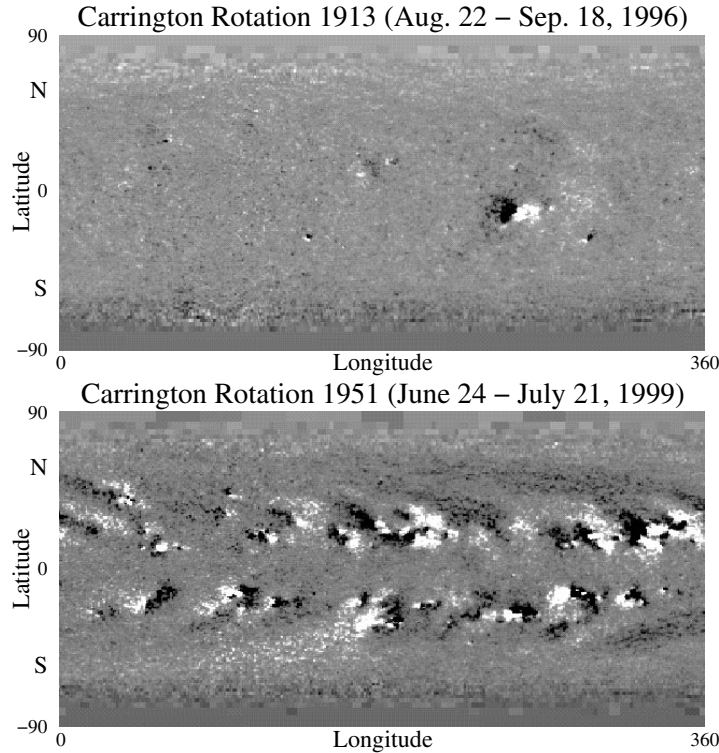


Figure 2. Synoptic maps of the radial component of the photospheric magnetic field near solar minimum (top) and approaching solar maximum (bottom).

density along the line of sight in the plane of the sky (convolved with a scattering function and filtered with a radial “vignetting function”).

On 6 August 1999 we performed an updated calculation using the most recent magnetic field measurements available from NSOKP on that day, to incorporate the evolution of the magnetic field. The measurements used in the synoptic map were those from 13 July–5 August, 1999 (the synoptic map included Carrington longitudes  $0^{\circ}$ – $107^{\circ}$  from Carrington rotation 1951 and  $107^{\circ}$ – $360^{\circ}$  from rotation 1952). Due to time constraints, the updated calculation was performed on a coarser grid ( $61 \times 71 \times 64$ ), and required 4 hours of CPU time. The results show that there are changes in the predicted coronal structure in the updated calculation. In particular, the position of some streamers changed perceptibly, and they had different tilts (especially near the west solar limb, where the magnetic field data was updated most significantly). However, the large-scale structure of the corona did not change dramatically. The updated calculation was not relaxed to steady state sufficiently, and the spatial resolution was inadequate, so that the results shown in this paper use the calculation with data for Carrington rotation 1951.

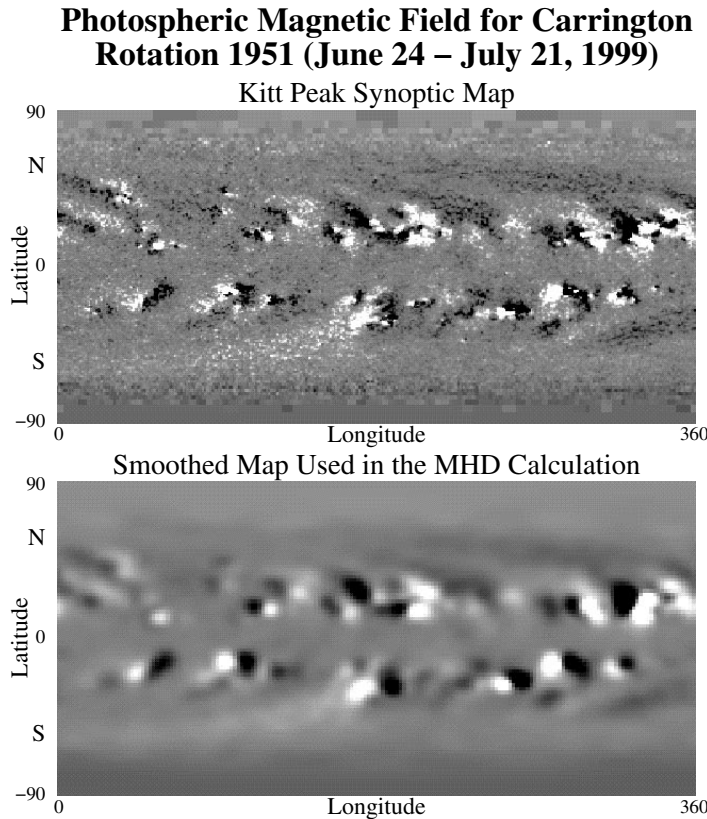


Figure 3. Synoptic map of the radial component of the photospheric magnetic field measured at the National Solar Observatory at Kitt Peak for Carrington rotation 1951 (top), and the smoothed version (bottom) that was used as a boundary condition for the MHD calculation for the eclipse prediction.

#### 4. Comparison with an Eclipse Image

NASA astronomer Fred Espenak photographed the total solar eclipse on 11 August 1999 from Lake Hazar, Turkey. Twenty-two separate images with different exposures were combined digitally into a single composite image that more closely resembles the appearance of the solar corona as seen by the human eye (Espenak 1999). Additional photographs of the eclipse can be found on Fred Espenak's eclipse World Wide Web site.<sup>3</sup>

Figure 4 shows this eclipse image, as well as our predicted polarization brightness ( $pB$ ) from the MHD model. The  $pB$  image was calculated from the simulated corona as it would appear in the plane of the sky on 11 August 1999, at 11:38 UT (corresponding to totality in Eastern Turkey), and has been radially detrended to account for the fall-off of coronal brightness with distance from the

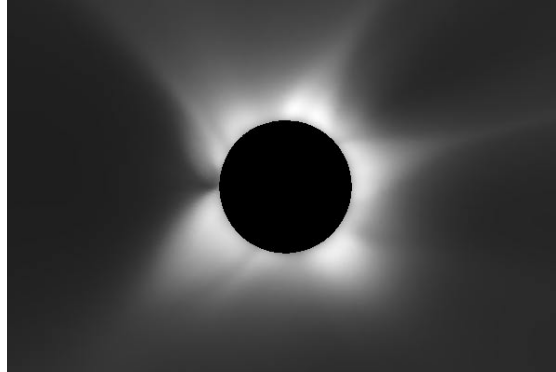
<sup>3</sup>See: <http://www.mreclipse.com/TSE99reports/TSE99Espenak.html>

### Comparison of a 3D MHD Coronal Prediction with an Image of the 11 August 1999 Total Solar Eclipse

Fred Espenak's Composite Image (Turkey)



Predicted Polarization Brightness (MHD Model)



Predicted Magnetic Field Lines (MHD Model)

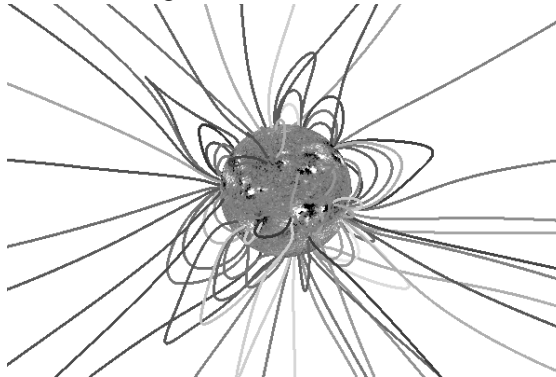


Figure 4. Comparison between a composite eclipse image created from photographs taken by Fred Espenak in Lake Hazar, Turkey (top) with the predicted polarization brightness of the simulated solar corona from our 3D MHD model (middle). The projected magnetic field lines from the model are also shown (bottom). Terrestrial (geocentric) north is vertically upward. (Solar north is  $15^\circ$  counterclockwise.) The eclipse image is copyrighted © 1999 by Fred Espenak.

Sun. This detrending is similar to the effect of combining various exposures in the composite eclipse image (although it is not an identical procedure), and is an attempt to reproduce the image seen by the human eye. Therefore, the agreement between the two images can only be expected to be qualitative at best; namely, the position and structure of streamers and coronal features ought to agree, but the brightness of individual features would not be expected to agree.

It is apparent that the eclipse image has considerably more fine structure than our prediction. This is primarily due to the limited spatial resolution of our calculation, but may also be due to the polytropic energy equation used in our model, and the fact that the fine-scale structure has been emphasized in the composite image (Esenak 1999). Note that the features that resemble “plumes,” that are visible in the eclipse image at equatorial latitudes on the east solar limb, are not present in the model.

Previous comparisons of our simulations with Mauna Loa MK3 coronagraph observations on several days surrounding our solar minimum eclipse predictions have confirmed that the basic large-scale three-dimensional structure of the streamer belt is captured in our model (Linker et al. 1999). However, the agreement between our prediction and eclipse images as we approach solar maximum is not as good. The principal discrepancy seems to be in the tilt of the helmet streamers, and in the fact that we miss individual streamers, especially in the polar regions. Possible reasons for this discrepancy are discussed in the next section. Overall, however, the prediction gives a fair approximation to the state of the large-scale solar corona.

It is difficult to portray the complex three-dimensional structure of the solar corona for this simulation using still images. It is best seen in a movie of the polarization brightness during the whole solar rotation (Carrington rotation 1951), which can be found at our Web site.<sup>4</sup>

## 5. Discussion

During solar maximum the solar magnetic field is changing rapidly as new active regions emerge daily and disperse as they interact with existing active regions. The accuracy of an equilibrium model, which is based on synoptic magnetic field measurements, such as the one we describe, is therefore expected to be limited. Not surprisingly, the match between the prediction and actual observations is poorer during this time of high solar activity than it was during solar minimum. Furthermore, the failure to match the transverse component of the magnetic field (which is presently not measured), which specifies the “shear” in the field, and consequently the energization level of the coronal field (Mikić & Linker 1997), is expected to be most severe at solar maximum when the magnetic field is generally most active (and hence significantly “energized”).

These two key approximations will be improved in future versions of our model. First, we now have the capability of running time-dependent simulations of the evolving solar corona as it responds to changes in the photospheric

---

<sup>4</sup>See: <http://haven.saic.com/corona/modeling.html>

magnetic field. In the future, we will be able to use daily magnetic field measurements to calculate the evolving solar corona. Second, current plans at Kitt Peak National Solar Observatory call for measurements of the vector magnetic field in the photosphere to be taken (the SOLIS project), which can be used in our model to match the transverse component of the magnetic field at the base of the corona (Mikić et al. 1999). A benefit of vector magnetic field measurements will be that polar fields will be more accurately determined (since the polar field, which is predominantly radial, will be measured as part of the transverse component). This can be expected to improve future predictions. Finally, our predictions will also be improved when our model with the more sophisticated energy equation becomes operational, and when we can perform higher-resolution calculations in less time with the massively parallel version of our code.

**Acknowledgments.** We wish to thank Dr. Jack Harvey at Kitt Peak National Solar Observatory for kindly providing us with up-to-date magnetic field data for our eclipse prediction. We thank Dr. Fred Espenak for use of his eclipse image. We thank Drs. Atila Özgüç and Tamer Atac for their hospitality and kindness during ZM's visit to Turkey. Kitt Peak synoptic magnetic data are courtesy of NSOKP, which is funded cooperatively by NSF/NOAO, NASA/GSFC, and NOAA/SEC. This research was supported by the NASA Space Physics Theory Program, the NASA Supporting Research and Technology Program, the NASA SOHO Guest Investigator Program, and NSF grant ATM-9613834. Computational facilities were provided by NSF at the San Diego Supercomputer Center.

## References

- Endler, F. 1971, Ph. D. Thesis, Gottingen University
- Espenak, F. 1999, in this volume
- Linker, J. A., & Mikić, Z. 1995, *ApJ*, 438, L45
- Linker, J. A., & Mikić, Z. 1997, in *Coronal Mass Ejections*, Geophysical Monograph 99, ed. N. Crooker, J. Joselyn & J. Feynman (American Geophysical Union), 269
- Linker, J. A., Mikić, Z., Biesecker, D. A., Forsyth, R. J., Gibson, S. E., Lazarus, A. J., Lecinski, A., Riley, P., Szabo, A., & Thompson, B. J. 1999, *J. Geophys. Res.*, 104, 9809
- Linker, J. A., Mikić, Z., & Schnack, D. D. 1994, in *Proc. Third SOHO Workshop, SP-373, Solar Dynamic Phenomena and Solar Wind Consequences*, Estes Park, Colorado, USA (European Space Agency), 249
- Linker, J. A., Mikić, Z., & Schnack, D. D. 1996, in *ASP Conf. Ser. Vol. 95, Solar Drivers of Interplanetary and Terrestrial Disturbances*, ed. K. S. Balasubramaniam, S. L. Keil & R. N. Smartt (San Francisco: ASP), 208
- Lionello, R., Mikić, Z., & Schnack, D. D. 1998, *J. Comput. Phys.*, 140, 172
- Mikić, Z., & Linker, J. A. 1994, *ApJ*, 430, 898
- Mikić, Z., & Linker, J. A. 1996, in *AIP Conf. Proc.*, 382, *Solar Wind Eight: Proc. of the Eight Intl. Solar Wind Conf.*, ed. D. Winterhalter, J. T.

- Gosling, S. R. Habbal, W. S. Kurth & M. Neugebauer (New York: AIP), 104
- Mikić, Z., & Linker, J. A. 1997, in *Coronal Mass Ejections*, Geophysical Monograph 99, ed. N. Crooker, J. Joselyn & J. Feynman (American Geophysical Union), 57
- Mikić, Z., Linker, J. A., Schnack, D. D., Lionello, R., & Tarditi, A. 1999, *Phys. Plasmas*, 6, 2217
- Parker, E. N. 1963, *Interplanetary Dynamical Processes* (New York: Wiley-Interscience)
- Pneuman, G. W., & Kopp, R. A. 1971, *Sol. Phys.*, 18, 258
- Steinolfson, R. S., Suess, S. T., & Wu, S. T. 1982, *ApJ*, 255, 730
- Suess, S. T., Wang, A.-H., Wu, S. T., Poletto, G., & McComas, D. J. 1999, *J. Geophys. Res.*, 104, 4697
- Usmanov, A. V. 1993, *Sol. Phys.*, 146, 377
- Usmanov, A. V. 1999, in *AIP Conf. Proc.*, 471, *Solar Wind Nine: Proc. of the Ninth Intl. Solar Wind Conf.*, ed. S. R. Habbal, R. Esser, J. V. Hollweg & P. A. Isenberg (New York: AIP), 397
- Wang, A. H., Wu, S. T., Suess, S. T., & Poletto, G. 1993, *Sol. Phys.*, 147, 55
- Washimi, H., Yoshino, Y., & Ogino, T. 1987, *Geophys. Res. Lett.*, 14, 487